Measurement of $2l$-nl' x-ray transitions from ≈ 1 μm Kr clusters irradiated by high-intensity femtosecond laser pulses

S. B. Hansen and K. B. Fournier
Lawrence Livermore National Laboratory, P.O. Box 808, L-473, Livermore, California 94550, USA

A. Ya. Faenov, A. I. Magunov, T. A. Pikuz, and I. Yu. Skobelev
Multicharged Ions Spectra Data Center of VNIIFTRI, Mendeleevo, Moscow region 141570, Russia

Y. Fukuda, Y. Akahane, M. Aoyama, N. Inoue, H. Ueda, and K. Yamakawa
Advanced Photon Research Center, Japan Atomic Energy Research Institute (JAERI), 8-1 Umemidai, Kizu-cho, Souraku-gun, Kyoto 619-0215, Japan

(Received 18 June 2004; published 14 January 2005)

X-ray line emission from $2l$-nl' transitions in Ne-like Kr and nearby ions has been observed from ≈ 1 μm Kr clusters irradiated by fs-scale laser pulses at the JAERI facility in Kyoto, Japan. The incident laser intensity reached 10^{19} W/cm^2, with pulse energies from 50 to 300 mJ and pulse durations from 30 to 500 fs. The dependence of the x-ray spectral features and intensity on the incident laser intensity is rather weak, indicating that the 1–2 ps cluster lifetimes limit the number of ions beyond Ne-like Kr that can be produced by collisional ionization. Lines from F- to Al-like Kr emitted from the cluster plasmas have been identified using data from the relativistic multiconfiguration flexible atomic code. A collisional-radiative model based on these data has been constructed and used to determine that the cluster plasma has electron densities near 10^{22} cm^{-3}, temperatures of a few hundred eV, and hot electron fractions of a few percent.

DOI: 10.1103/PhysRevE.71.016408 PACS number(s): 52.50.Jm, 32.30.Rj, 36.40.Vz, 52.25.Os

I. INTRODUCTION

Plasmas formed by the irradiation of gas clusters by short-pulse, high-intensity lasers [1] are promising x-ray emission sources and have been extensively studied over the last few years [2–7]. Resonant laser-plasma interactions within cluster targets generate high-energy particles [2,3] such as hot electrons, which can lead to considerable x-ray yields [4–7]. The study of cluster targets under intense laser irradiation is relevant to fusion studies [2], development of high-intensity x-ray sources [1], and investigations into the behavior of matter in ultrahigh electric fields [8].

The interaction of ultrashort laser pulses with solid targets can generate plasmas with very high electron densities [9] and significant fractions of hot electrons [10,11], but the conversion efficiency of laser light to multi-keV x rays from solid targets tends to be rather low. The absorption of laser light by a uniform low-density gas is inherently more efficient than by a massive, solid target [12,13] because the laser can supersonically ionize and heat large volumes with little or no loss of energy to ablative interactions with the target far from the emitting region. For this reason, gas cluster targets [8] and low-density solid targets [14] are also efficient absorbers of laser energy.

In a previous work [5], the $2l$-$4l'$ emission from Ne-like Kr and surrounding ions was analyzed and used to diagnose the conditions of ≈ 0.1 μm clusters irradiated by 60 and 500 fs laser pulses with 4–15 mJ of energy and intensities of a few times 10^{17} W/cm^2. Those plasmas contained hot, dense regions consisting of cluster remnants with electron densities near 10^{21} cm^{-3}, temperatures between 300 and 400 eV, and hot electron fractions of 2-4 %. The cluster plasma regions from which most of the L-shell x rays were emitted were surrounded by cooler (200 eV), rarer (10^{20} cm^{-3}) plasma formed during the laser prepulse.

In the present work, emission from $2l$-nl' transitions with $n \leqslant 6$ is analyzed from larger Kr clusters whose dimensions are estimated to be ≈ 1 μm. The nozzle in this experiment was designed to maximize the cluster size [15], since larger clusters have been found to be less susceptible to destruction by the laser prepulse and more efficient absorbers of the laser energy [5]. The large Kr clusters in the present experiment were irradiated by 30–500 fs laser pulses with 50–300 mJ of energy; laser intensities up to 10^{19} W/cm^2 have been achieved. The resulting L-shell Kr emission spectra indicate that the cluster plasmas reach electron densities larger than 10^{22} cm^{-3}, have temperatures near 250 eV, and hot electron fractions near 2%. We estimate that absorption efficiencies between 10 and 50 % are required to produce the diagnosed conditions in the cluster plasmas.

Previous measurements of $2l$-nl' emission from O- to Mg-like Kr (with $n \leqslant 9$) have been performed with a low-density tokamak plasma [16] and analyzed using theoretical data from the well-established RELAC code [17]. In the present work, data calculated with the flexible atomic code (FAC) [18], a new relativistic multiconfiguration atomic structure code, are used to identify emission features from F- to Al-like Kr in Kr cluster spectra. Experimental data have been collected in two spectral regions encompassing 4–2 and higher Rydberg transitions (5.2-5.8 and 4.6–5.2 Å, respectively). Details of the experiment and a summary of the experimental results are given in Sec. II below. In Sec. III, a collisional-radiative model of O- to Si-like Kr that includes self-consistent opacity and hot electron effects is described

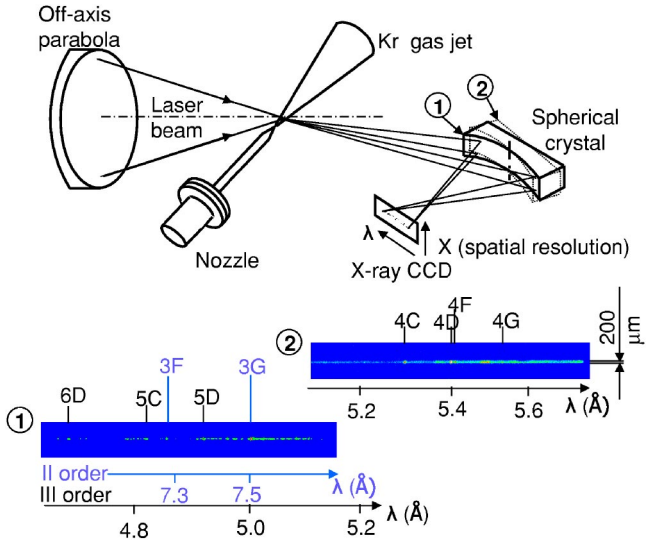

FIG. 1. (Color online) Experimental setup, including laser, gas jet nozzle and target, and FSSR-2D spectrometer. Two alignments of the spherical mica crystal (numbered 1 and 2) were used to measure x-ray emission from two different spectral regions; spectra from these regions are given in the bottom panel. In alignment 1, the mica spectrometer captured $2p$-$3s$ emission in second order as well as higher Rydberg emission.

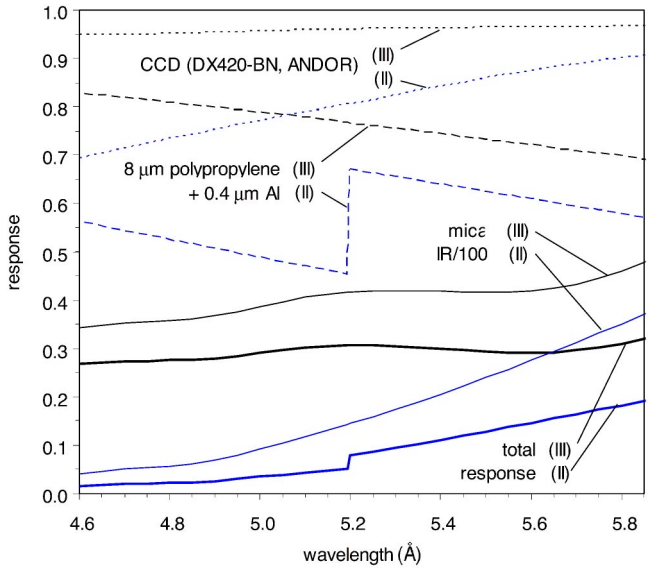

FIG. 2. (Color online) Filter and CCD detector responses and integrated reflectivities (IR) of mica in the second and third reflection orders. (The plotted reflectivity values are IR/100 taken from experimental data given in Ref. [27,28].) The total response of the detection system is also given for both orders.

and used to diagnose the size, density, temperature, and hot electron fractions of the cluster plasmas from the measured x-ray emission spectra. A discussion is given in Sec. IV and a summary is given in Sec. V.

II. EXPERIMENTAL SETUP AND RESULTS

The experiments were performed with the JAERI (Kyoto, Japan) 100 TW Ti:sapphire laser system, which is based on the technique of chirped pulse amplification. The laser was designed to generate 20 fs pulses centered at 800 nm at a 10 Hz repetition rate and is capable of producing focusing intensity up to 10^{20} W/cm^2 [19–21]. In this study, the amplified pulses were compressed to 30–500 fs by a vacuum pulse compressor yielding a pulse energy of 320 mJ. The pulses go through a regenerative amplifier and then through two double Pockels cells to reduce the prepulse, which comes before the main pulse by 10 ns. In this way, a contrast ratio of 5×10^{-6} between the intensity of the main pulse and the prepulse is achieved [21]. In a vacuum target chamber, the compressed pulses were focused by an $f/3$ Au-coated off-axis parabolic mirror. The measured spot size was 11 μm at $1/e^2$, which is 1.1 times larger than the diffraction limit. Approximately 64% of the laser energy was contained in the 11 μm Gaussian spot.

Figure 1 shows the experimental setup of the laser, gas jet nozzle and target, and spectrometer. The Kr clusters were produced by expanding a high pressure (20–30 atm) Kr gas into vacuum through a specially designed pulsed conical nozzle: the input and output diameters of the nozzle were 0.5 and 2.0 mm, respectively, and its length was 75 mm. The parameters of the nozzle were obtained from numerical modeling of a cluster target using the hydrodynamic code developed at the Institute of Mathematical Modeling (RAS) [6,15,22]. By using the specially designed nozzle, Kr clusters with an average diameter around 1 μm can be produced at the laser focal spot (about 1.5 mm downstream from the nozzle). Such large clusters are less susceptible to destruction than the $\approx$0.1 μm Kr clusters produced in previous experiments [5]. While the RAS model's predictions for mean cluster size and cluster concentration for argon gas clusters at backing pressures of 20–60 bars have given quantitative agreement with experiment [23], its predictions for the size of the present clusters have not been independently verified. However, we show below that the predicted cluster size and concentration are consistent with the observed opacities and the measured plasma emission dimension.

Spatially resolved x-ray spectra were measured using an focusing spectrometer with spatial resolution (FSSR-2D) [24–26]. This spectrometer has been equipped with a spherically bent mica crystal (R=150 mm) and a vacuum-compatible x-ray charge-coupled device (CCD) camera (DX420-BN, ANDOR), which was filtered with 8 μm of polypropelyne and 0.4 μm of Al. The spherically bent mica crystal was placed 381.2 mm from the plasma source and centered at λ=5.4 Å (corresponding to the Bragg angle θ =54.3° for the third reflection order of the mica crystal) in order to observe 4-2 transitions in Kr. To observe higher Rydberg lines, the crystal was slightly shifted to 360 mm to obtain a central wavelength of λ=4.82 Å (with a Bragg angle of θ=46.5°). The filter and CCD detector responses (efficiencies) of the detection system and the integrated reflectivities of mica [27,28] are given in Fig. 2 across the two spectral regions for both second and third order emission. Even though much of the second order emission is filtered out, some $2p$-$3s$ emission is evident in the high-Rydberg spectral region (see Figs. 1 and 3).

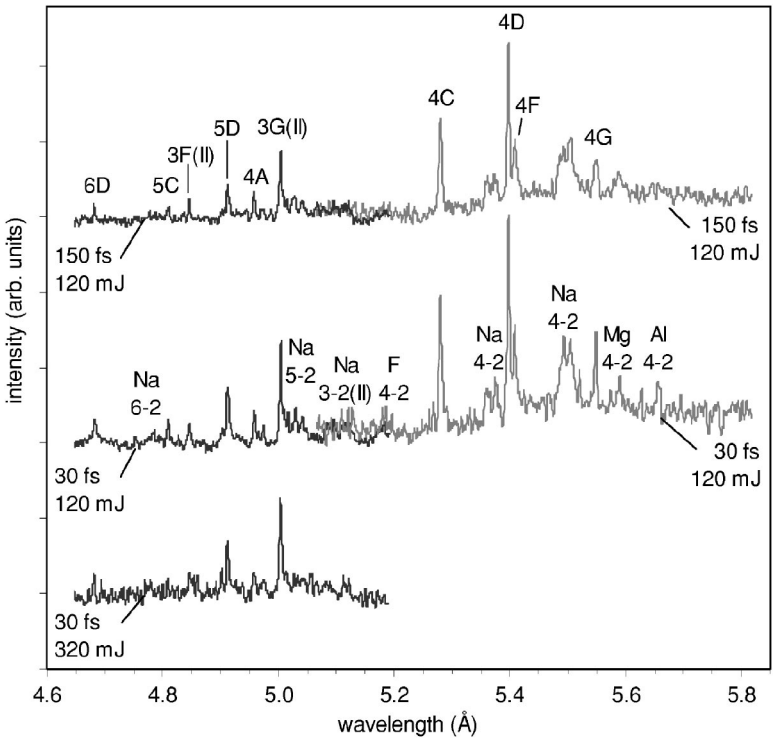

FIG. 3. Measured spectra of *nl*-2*l*′ Kr emission from experiments with various laser energies and durations, with the incident laser intensities increasing from top to bottom. Ne-like Kr lines are labeled with their common designations and satellite features are labeled with their parent ion and the principal quantum numbers of the dominant transitions.

The reflection plane of the spectrometer was oriented along the direction of the laser beam propagation to obtain spatial resolution in the transverse direction. The measured size of the emission zone in that direction was 200–250 μm. The emission zone in the direction of laser propagation was estimated to be between 1.0 and 1.5 mm. As the spectrometer crystal had a spherical shape and was placed on the Rowland circle, the spectral resolution was not sensitive to the size of the plasma source and approached the limit of the x-ray CCD camera detector ($\lambda/\Delta\lambda \approx 7000$).

Figure 3 shows measured spectra from each of the two alignments of the spectrometer for experiments with laser energies from 120 to 320 mJ and pulse durations from 30 to150 fs. The relative spectral line intensities are proportional to the measured counts on the CCD. The top two spectra combine data from two experiments with the same laser parameters (120 mJ and durations of 150 and 30 fs) and different crystal alignments; the bottom spectrum shows only data in the high-Rydberg region for a 320 mJ, 30 fs laser pulse (no data were taken with the 4-2 crystal alignment for these laser parameters). The highly resolved Ne-like lines are labeled with with their common designations *nX*, where *n* is the principal quantum number of the upper level and *X* specifies the transition type (*n*A and *n*B are *np*-2*s*, *n*C and *n*D are *nd*-2*p*, and *n*F and *n*G are *ns*-2*p*). Other spectral features are labeled with their parent ions and the principal quantum numbers of the dominant transitions. The wavelengths were calibrated using experimental values from [16] for the Ne-like *n*C and *n*D Kr lines, which agree with wavelengths calculated using the atomic structure code FAC [18] to within 6 mÅ.

Although the laser intensity increases over an order of magnitude from top to bottom in Fig. 3, the measured spectra exhibit fairly little variation in their emission features. This near uniformity suggests that the plasma conditions attained in the clusters are only weakly affected by the laser parameters. Figure 4 shows experimental intensities of the 4D and 5D lines compiled from 18 experiments with various laser energies and durations. The data have a fair level of reproducibility and exhibit general trends of increasing emission intensity with increasing laser energy and decreasing laser duration. This dependence of x-ray emission intensity on the incident laser intensity, while rather weak, could be due either to variations in the plasma conditions reached in the clusters or to a variations in the number of emitting ions. These two possibilities are discussed in the modeling section below.

III. MODELED SPECTRA AND COLLISIONAL-RADIATIVE DIAGNOSTICS

The emission lines and features in the experimental Kr spectra were identified and calibrated with theoretical data calculated using the new relativistic multiconfiguration atomic structure code FAC [18]. The data include level energies, radiative and Auger decay rates, collisional excitation and ionization cross sections, and radiative recombination cross sections for fine structure levels within O- through Si-like Kr. Table I lists the configurations and number of fine structure levels included in the calculations for each ion.

There are thousands of radiative transitions between levels in the listed configurations in the wavelength region from 4.6 to 5.8 Å. These have been separated according to their parent ion and plotted with intensities given by statistically weighted radiative decay rates in Fig. 5. In this figure, the wavelength region is separated into high-Rydberg transitions (top) and 4-2 transitions (bottom). Note that the radiative decay rates of similar transitions are quite uniform for ions

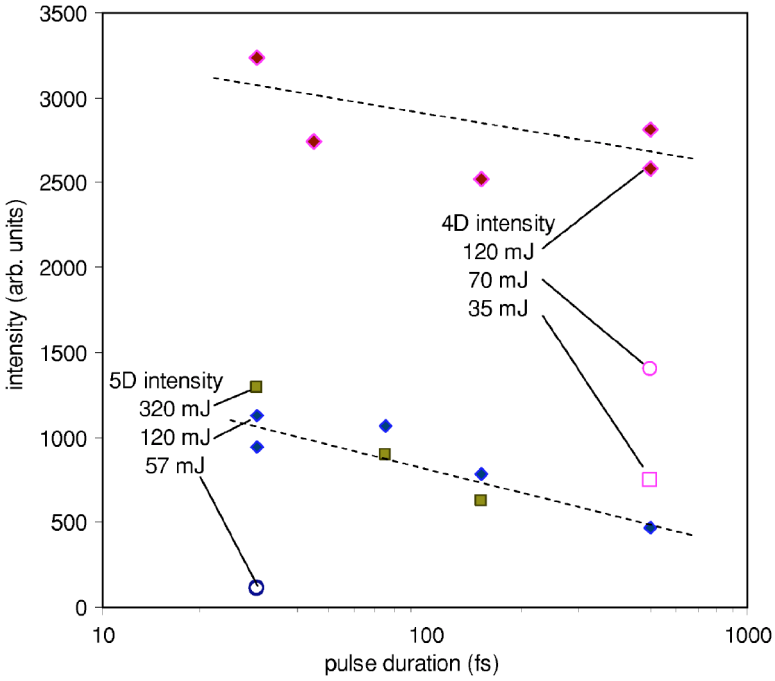

FIG. 4. (Color online) Variation with laser pulse duration and energy of the measured intensities of Ne-like 4D and 5D lines. The x-ray emission intensities tend to increase with laser energy and decrease with increasing pulse duration.

from O- to Si-like Kr. For clarity, the 3-2 features that appear in second order in the experimental spectra are not included in this figure; they consist mainly of the 3F and 3G Ne-like lines and associated Na- and Mg-like satellites.

A. Collisional-radiative model

A collisional radiative (CR) model based on the FAC data has been constructed to diagnose the cluster plasma conditions. A set of collisional-radiative rate equations are generated which include collisional excitation and de-excitation, collisional ionization, three-body recombination, dielectronic capture, Auger decay, radiative recombination, and radiative decay. The collisional rates are calculated using an electron distribution function characterized by an electron density n_e, a bulk electron temperature T_e, and a fraction of hot electrons f. Hot electrons are generated by resonant interactions between the main laser pulse and electrons that exist in a relatively cool plasma formed in the clusters by the laser prepulse [4–7]. Using the semiempirical formulation given in Ref. [29], the laser parameters of the present experiment point to characteristic hot electron energies of 20–100 keV. In this work, we model the hot electron distribution using a narrow Gaussian centered at 20 keV. (In our previous work with Kr clusters [5], the laser intensity was much smaller and we modeled the hot electrons with a 5 keV Gaussian beam.)

TABLE I. Configurations included in the collisional-radiative model and the number of fine-structure levels in each ion. Energies and rates coupling the levels have been calculated using the atomic structure code FAC [18].

Ion	Configuration	Num. levels
O	$2s^22p^4$, $2s2p^5$ $2s^22p^3nl$, $2s2p^4nl$ $(n\leqslant 5)$	879
F	$2s^22p^5$, $2s2p^6$ $2s^22p^4nl$, $2s2p^5nl$ $(n\leqslant 5)$	480
Ne	$2s^22p^6$ $2s^22p^5nl$, $2s2p^6nl$ $(n\leqslant 6)$	241
Na	$2s^22p^6nl$ $(n\leqslant 6)$ $2s^22p^53lnl'$, $2s2p^63lnl'$ $(n\leqslant 4)$ $2s^22p^53lnd$ $(n\leqslant 6)$	1410
Mg	$2s^22p^63lnl'$ $(n\leqslant 4)$ $2s^22p^53s3lnd$ $(n\leqslant 4)$	707
Al	$2s^22p^63s^23p$ $2s^22p^63s^2nd$ $(n\leqslant 4)$ $2s^22p^53s^23lnd$ $(n\leqslant 4)$	277
Si	$2s^22p^63s^23p3l$ $2s^22p^63s^23l4d$ $2s^22p^53s^23pnd$ $(n\leqslant 4)$	363

The effects of hot electrons on x-ray emission spectra from ultrashort laser plasmas have been much studied in recent years, and a variety of distributions for the hot electrons have been implemented. Extensive modeling of *K*-shell emission from Ar clusters used a Gaussian distribution centered at 5 keV to describe hot electrons [4,6] and modeling of *L*-shell emission from solid Cu and Zn targets used Maxwellian distributions with T_{hot}=5 keV [10,11]. It has long been observed that when hot electrons are modeled by a narrow Gaussian distribution, the central energy of the Gaussian has a relatively small effect on the calculated collisional rates [30–32], and a similar insensitivity to the hot electron temperature has been noted when Maxwellian distributions are used [11]. Recently, these conclusions have been generalized [33] to show that neither the characteristic (central or average) energy nor the exact functional form of the hot electron distribution has a large effect on the collisional rates as long as the characteristic energy is larger than the most energetic transition of interest. Since inner-shell excitations of 1*s* electrons in near-neonlike Kr ions with ener-

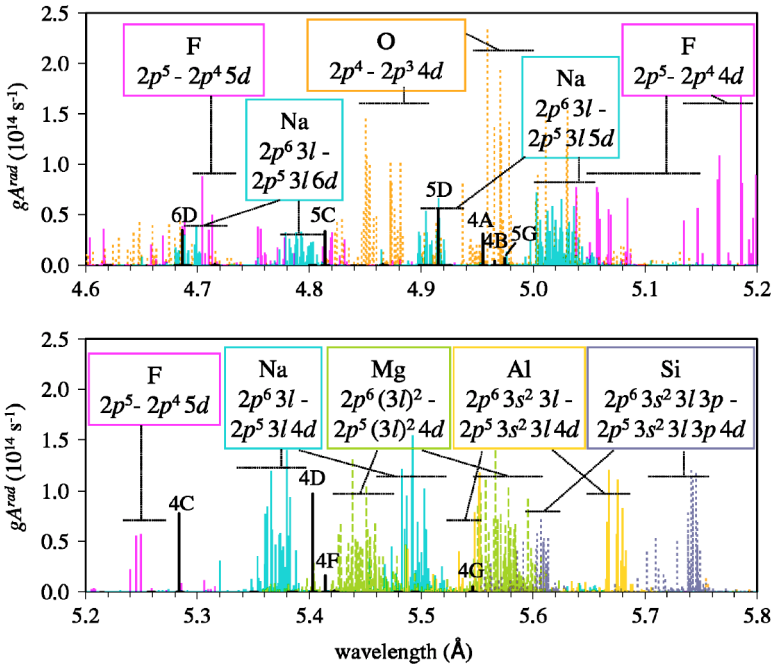

FIG. 5. (Color online) Statistically weighted radiative decay rates (gA^{rad}) of high Rydberg *nl* -2*l*′ (top) and 4*l*-2*l*′ (bottom) transitions from O- to Si-like Kr. The features are labeled with their parent ion and the dominant transition type.

gies of 12–15 keV are possible, we use a hot electron energy above that excitation threshold. Such energetic inner-shell emission has recently been observed from ≈0.1 μm Kr clusters irradiated by 60 fs, ≈10^{18} W/cm^2 laser pulses [34].

Once collisional rates are calculated, a set of coupled collisional-radiative rate equations is obtained and solved in the steady-state approximation. Opacity effects on the level populations are included self-consistently using the escape factor formalism, an iterative procedure which uses the level populations from one iteration to generate escape factors that modify the rate equations for the next iteration. The escape factors account for self-absorption and stimulated emission as photons from individual transitions are transported across the plasma, and the rate equations modified by these processes are solved and re-modified until a self-consistent solution is reached.

Once level populations are determined, modeled spectra are constructed using Voigt profiles whose Doppler widths are dependent on the ion temperature (which is taken to be equal to T_e) and instrumental broadening and whose Lorentz widths are determined by the total rates of spontaneous and collisional depopulation from the upper and lower levels of each transition. Using the slab approximation to account for opacity effects on line intensities and profiles, the modeled spectral intensity at a frequency ν is given by

$$I(\nu) = \frac{j(\nu)}{\kappa(\nu)}\{1 - e^{-\kappa(\nu)d}\}, \tag{1}$$

where $j(\nu)$ and $\kappa(\nu)$ are, respectively, the total emissivity and absorptivity of the plasma at the photon frequency ν, and d is the effective plasma size (for more details, see Ref. [35]). In the present case, where numerical modeling [15] indicates that the ≈1 μm dense clusters are surrounded by ≈10 μm of rarer plasma, d effectively includes only the cluster portion of the plasma, whose dimensions can be estimated to be ≈1/10th the total plasma size.

The emission intensity given by Eq. (1) above is modulated by the detector response given in Fig. 2 in order to match the modeled spectra to measured data and thereby to diagnose the cluster plasma conditions. Following the results of Ref. [5], we assume the cool, rare plasma that surrounds the hot dense clusters makes relatively small contributions to the plasma emission and absorption. In fact, the main difference between the spectra in this work and the spectra from the smaller clusters in Ref. [5] is that the satellite emission from Mg-like and lower charge states of Kr is less intense than in the previous work, where including satellite emission from the rare plasma was necessary to obtain good agreement with the data. Since no such inclusion is found to be necessary here, the radiating clusters in the present experiment are likely to be either larger or more dense (or both) than those in the previous experiment. A second important difference between this work and Ref. [5] is that the smaller measured spectral range of only 4-2 transitions in Ref. [5] did not contain sufficient information for an independent determination of the electron density. In the present work, the wider spectral range and the presence of emission from two reflection orders contains sufficient information to independently determine n_e, T_e, f, and the total size of the dense cluster plasma d.

B. Variation of modeled spectra with plasma conditions

Figure 6 illustrates how changing the modeled plasma conditions affects the modeled spectra. In Fig. 6(a), the effects of varying the optical depth are shown. The optically thin spectrum, given in the bottom panel of Fig. 6(a), has a 4F/4D ratio which is far smaller than the experimental value shown in Fig. 3. Because the radiative decay rates of 4C and 4D are large compared to those of the higher Rydberg tran-

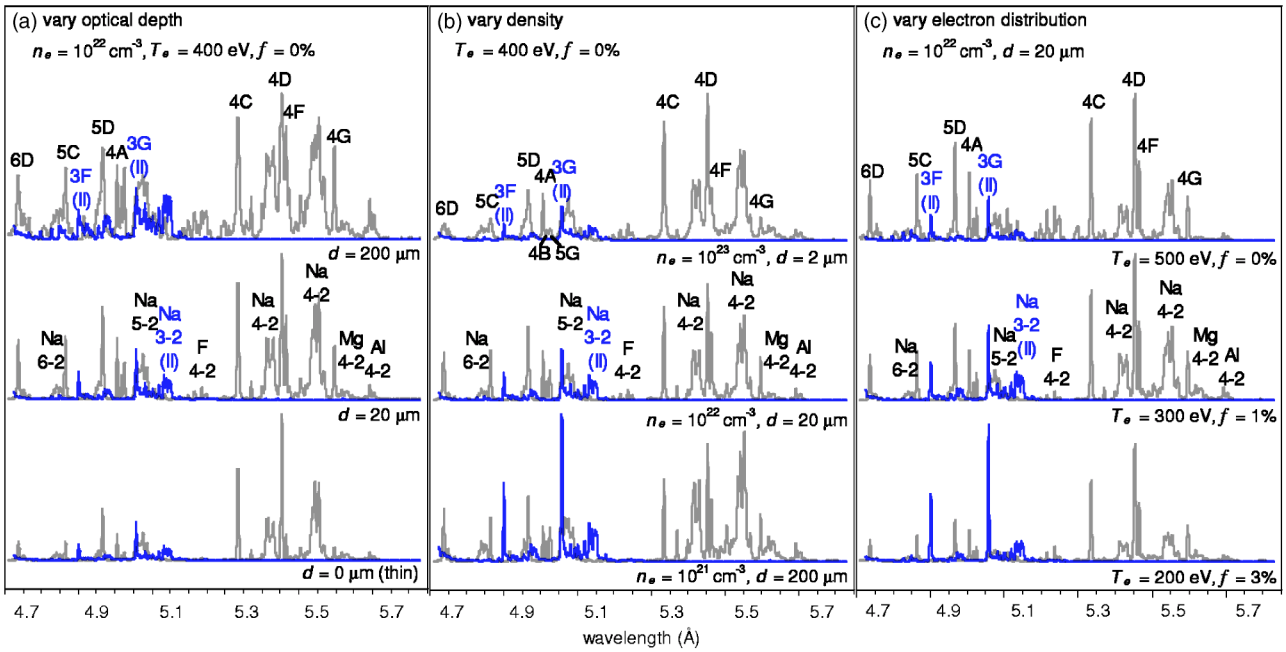

FIG. 6. (Color online) Modeled spectra of nl-$2l'$ Kr emission at various plasma conditions (including the total response of the detection system given in Fig. 2). Second (3-2) and third order emission (gray lines) are given separately.

sitions (see Fig. 5), the 4C and 4D lines are strongly affected by self-absorption at moderate optical depths. When self-consistent opacity effects are included for an effective (total) cluster size of 20 μm, the 4F/4D ratio increases to about the experimental value, and when a larger effective cluster size of 200 μm is modeled, as in the top spectrum of Fig. 6(a), the intensities of the 4F and 4G lines become too large to match the experimental spectra. The ratio 4F/4D is not much affected by variation of other plasma parameters (except by very high densities, which we will discuss below) so by fixing the ratio 4F/4D to match the experimental data, the optical depth can be firmly established, and the product $n_e \times d$ can be fixed to simplify the determination of n_e, T_e, and f. Note that the radiative decay rates of the $2p$-$3s$ transitions 3F and 3G are smaller than those of any $2p$-nd transitions in this wavelength range, making those lines fairly insensitive to opacity effects.

Figure 6(b) shows the effects of varying the electron density from 10^{21} to 10^{23} cm^{-3} while keeping the product $n_e \times d$ constant. The most obvious effect of this variation is the decrease in the intensities of the 3-2 3F and 3G lines with increasing n_e. The enhancement of the low-lying 3F and 3G lines due to increased radiative cascades as electron densities decrease is a well-known effect [36] that has been used to diagnose electron densities in laser [9] and X pinch plasmas [37,38]. Even considering variations in f which can also affect the 3-2 line intensities, the electron density in the clusters must be above $\approx 5 \times 10^{21}$ cm^{-3} to match the experimental data. Another feature which can help to pin down the electron density is the complex of the 4A, 4B, and 5F lines between 4.95 and 5.0 Å. The relative intensity of the 4A line to 4B and 5F increases substantially with the electron density and only matches the experimental data for densities above about 10^{22} cm^{-3}. Finally, the top spectrum in Fig. 6(b) shows that very high densities (above about 5×10^{22} cm^{-3}) are precluded because of density effects on the line structure surrounding the high-Rydberg 5D and 6D lines. In the experimental spectra, the 5D and 6D lines are fairly narrow and well defined. With increasing density, the Na-like satellite emission near these lines increases and makes them appear broader than in the experiment. Since this effect would be amplified at the high optical depths required to bring the 4F/4D ratio (which decreases at very high densities) into agreement with the experiment, the 4F/4D ratio is indeed a robust diagnostic of the optical depth for the present experimental spectra.

Having fixed the effective optical depth and determined a region of allowable n_e from about 1 to 5×10^{22} cm^{-3}, we can now turn to the diagnosis of the electron temperature T_e and hot electron fraction f. The effects of varying the electron distribution function while maintaining an ionization balance near Ne-like Kr are shown in Fig. 6(c). The high-temperature spectrum without hot electrons deviates from the two spectra with hot electrons in several ways which are typically evident in both K- and L-shell spectra [33]: Including hot electrons leads to emission from a larger number of ions, amplifies certain high-energy lines within satellite features, and increases the intensities of the cascade-fed 3-2 lines. Only the last effect is convolved with electron density effects, and since the spectra in Fig. 6(c) are modeled at the low end of the constrained density range discussed above (where 3F and 3G are as large as they can be due to pure density effects), hot electrons are required to produce the observed intensities of the 3F and 3G lines.

Thus the product of plasma size and density is determined by fitting the 4F/4D ratio to the experimental data, n_e is determined by fitting the structure of the 4A, 4B, and 5G complex, and finally, the electron temperature and hot elec-

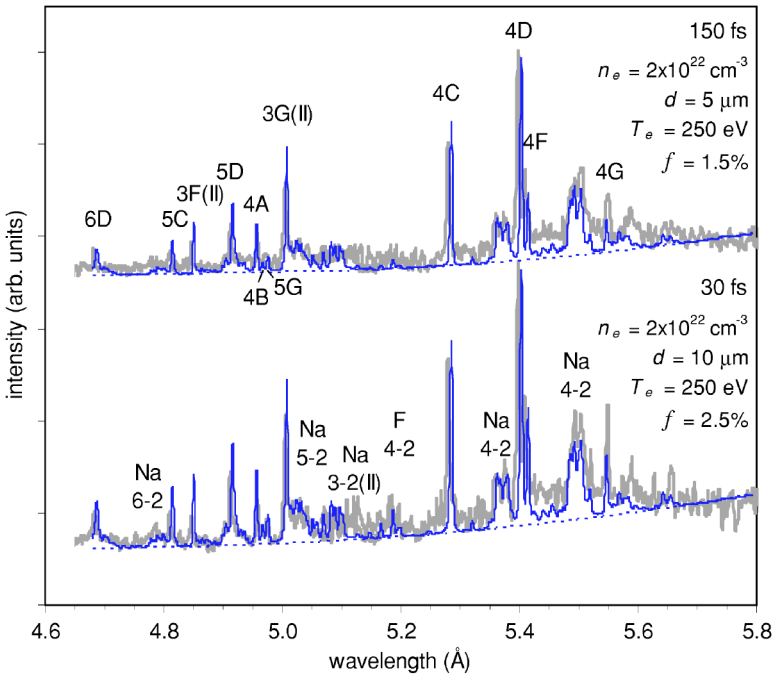

FIG. 7. (Color online) Comparison of experimental data (gray lines) with modeled spectra at the given plasma conditions. The energy of the laser pulse in each case was 120 mJ and the pulse duration varies from 150 fs (top) to 30 fs (bottom).

tron fraction are determined by fitting the 3-2 line intensities and the observed ionization balance. In this way, good fits to the experimental data can be achieved by varying only the four parameters T_e, f, n_e, and d. (As noted above and in Ref. [33], the functional form and exact energy of the hot electron distribution have only a small effect on the modeled spectra as long as the hot electron energy is sufficiently large.) This procedure can be used to isolate the density, plasma size, and hot electron fraction to within about a factor of 2 and the electron temperature to within about 30%. A demonstrably unique determination of the parameters with higher precision is difficult to obtain; this kind of multidimensional optimization problem is well suited for treatment by genetic algorithms, which can efficiently explore a complex parameter space [35,39].

C. Comparison of modeled to experimental spectra

Figure 7 shows comparisons of the best-fit modeled spectra with experimental data. The top spectrum of Fig. 7, from Kr clusters irradiated by 120 mJ and 150 fs laser pulses, has a 4F/4D ratio that implies somewhat smaller opacity effects than were shown in the middle spectrum of Fig. 6(a). With an effective plasma size of 5 μm and an electron density of 2×10^{22} cm^{-3}, the 4F/4D ratio and the relative intensities of the 4A, 4B, and 5G lines are fit very well. With a bulk electron temperature of 250 eV and f=1.5%, the satellite features, 3-2 line intensities, and the charge state balance of the modeled spectrum match the experimental data quite closely.

The lower spectrum in Fig. 7 is also from clusters irradiated with 120 mJ of energy, but with a shorter pulse duration (30 fs). Although the incident laser intensity is five times larger in this case than in the 150 fs spectrum, the intensity of 4D increases by a factor of only ≈1.7. As previously noted, this relatively modest change in the emitted x-ray intensity could be caused either by changes in the plasma conditions or by changes in the number of radiating ions. Our spectroscopic analysis suggests that both effects can play a role; the spectrum from the 30 fs laser pulse is best fit with the same temperature and density used to model the 150 fs spectrum, but with a larger fraction of hot electrons (2.5%) and a larger dimension (10 μm). These changes to the parameters not only increase the intensity of the modeled emission, but also increase the relative intensity of the *F*-like features near 5.2 Å and bring the 4F/4D ratio into agreement with the experimental data.

In fitting the time-integrated spectra with modeled emission at a single set of plasma conditions, we have assumed that the plasma conditions are static over the period of maximum emission. However, the Kr cluster plasma is inherently dynamic. Cluster expansion is one of the determining factors as to whether x rays are observed at all, since the size and density of the clusters at the time of the main laser pulse constrain the absorption of the laser energy. If the Kr clusters expand by a factor of 2 while they radiate during the few ps after the main laser pulse and before the clusters are completely dissolved, their density will fall by a factor of 8, so the time-integrated spectra must be considered as a sum over emission from time-varying plasma conditions. Since the x-ray emission intensity from each ion is strongly tied to the electron density and hot electron fraction through collisional excitation rates, the plasma conditions diagnosed from the available time-integrated data are weighted towards times at which the cluster plasma has the highest densities and largest hot electron fractions. This weighted estimate of the cluster plasma conditions is the most robust information we can obtain without time-resolved experimental data.

IV. DISCUSSION

The modeled spectra given in Fig. 7 fit the experimental data quite well and give plasma parameters that are consis-

tent with experimental constraints: Mathematical modeling of the Kr clusters estimates the cluster diameters to be ≈ 1 μm and the distance between clusters to be ≈ 10 μm. Since the clusters radiate after some attenuation by the laser prepulse but before they are completely destroyed, their effective size should be less than ≈ 20 μm, (1/10th the total plasma size of 200 μm; see Fig. 1). This is consistent with the diagnosed effective plasma size of 5–10 μm. The energy required to form the radiating plasma at the diagnosed conditions is also consistent with experimental constraints: Taking the cluster plasma to be a cylinder of length 150 μm and diameter 5–10 μm, and assuming a neutral plasma ($n_i = n_e/\langle Z \rangle$), there are $2-10 \times 10^{12}$ ions in the hot, dense cluster plasma at the diagnosed density. Since ≈ 30 keV ($\approx 5 \times 10^{-12}$ mJ) is required to ionize each Kr ion to the Ne-like charge state and heat the ionized electrons to the conditions in the diagnosed electron distribution, the cluster plasma requires 10–50 mJ from the 120 mJ laser pulse, implying absorption efficiencies up to 42%.

The fairly weak variation of the measured x-ray intensities and spectroscopic features with order-of-magnitude changes in the incident laser intensity is a somewhat unexpected result, indicating that something other than the incident laser characteristics acts as a constraint on the x-ray generation and charge state balance in the cluster plasmas. This additional constraint may be the time scales available for ionization and x-ray production, which are limited by the time it takes the clusters to expand beyond the density at which collisions can efficiently excite and ionize the Kr ions. Indeed, while ionization from Na- to Ne-like Kr has a time scale of a few ps under the diagnosed plasma conditions, ionization of the stable Ne-like ion to F-like Kr takes about ten times longer. Since the large, ≈ 1 μm clusters dissipate in ≈ 2 ps, ionization stages much higher than Ne-like Kr may not be attainable even at ultrahigh laser intensities. However, since hot electrons are present in the cluster plasmas, inner-shell excitation of Ne-like Kr and surrounding ions can take place, as demonstrated in Ref. [34]. And since cluster size has a significant impact on the plasma evolution [3], the constraint imposed by collisional ionization may not apply if even larger clusters with longer lifetimes could be produced.

V. SUMMARY AND CONCLUSIONS

X-ray emission from nl-$2l'$ transitions in F- to Al-like Kr has been measured from Kr clusters irradiated with laser intensities up to 10^{19} W/cm^2. The incident laser intensities have been varied over an order of magnitude by changing the energy and duration of the laser pulse, and a general trend of decreasing x-ray emission intensity with increasing laser pulse duration and decreasing laser energy has been observed. However, these trends are fairly small, and the emission features present in the measured emission spectra also change little over wide variations in laser intensity. The observations suggest that time constraints imposed by cluster expansion may limit the charge state balance regardless of the incident laser intensity.

The emission lines in the measured spectra have been identified and modeled using data from the new multiconfiguration relativistic atomic structure code FAC, which has proven to be a reliable theoretical tool. The conditions of the Kr cluster plasmas have been diagnosed using a collisional-radiative model that includes self-consistent opacity and hot electron effects. The diagnosed electron densities are significantly higher than those in ns-laser and previous experiments performed with lower incident laser intensities and smaller clusters, as predicted in Ref. [5].

ACKNOWLEDGMENTS

This work was supported in part by the Russian Foundation for Basic Research (Grant No. 02-01-00708), INTAS (Grant No. 01-0233), and by Grant No. RP1-2328-ME-02 of the U.S. Civilian Research and Development Foundation for the Independent States of the Former Soviet Union (CRDF). The work of S.H. and K.F. was performed under the auspices of the U.S. Department of Energy at University of California Lawrence Livermore National Laboratory under Contract No. W-7405-Eng-48.

[1] A. McPherson *et al.*, Phys. Rev. Lett. **72**, 1810 (1994).
[2] T. Ditmire *et al.*, Nature (London) **398**, 489 (1999).
[3] H. M. Milchberg, S. J. McNaught, and E. Parra, Phys. Rev. E **64**, 056402 (2001).
[4] G. C. Junkel-Vives *et al.*, Phys. Rev. A **66**, 033204 (2002).
[5] S. B. Hansen *et al.*, Phys. Rev. E **66**, 046412 (2002).
[6] G. C. Junkel-Vives *et al.*, Phys. Rev. E **65**, 036410 (2002).
[7] J. Abdallah, Jr. *et al.*, Phys. Rev. A **68**, 063201 (2003).
[8] Y. Fukuda *et al.*, Phys. Rev. A **67**, 061201(R) (2003).
[9] B. K. F. Young *et al.*, J. Quant. Spectrosc. Radiat. Transf. **58**, 991 (1997).
[10] K. B. Fournier *et al.*, J. Quant. Spectrosc. Radiat. Transf. **81**, 167 (2003).
[11] K. B. Fournier *et al.*, Phys. Rev. E **67**, 016402 (2003).
[12] J. Denavit and D. W. Phillion, Phys. Plasmas **1**, 1971 (1994).
[13] C. A. Back *et al.*, Phys. Plasmas **10**, 2047 (2003).
[14] K. B. Fournier *et al.*, Phys. Rev. Lett. **92**, 165005 (2004).
[15] A. S. Boldarev, V. A. Gasilov, and A. Ya. Faenov, Zh. Tekh. Fiz. **74**, 10 (2004) [Tech. Phys. **49**, 388 (2004)].
[16] J. E. Rice *et al.*, J. Phys. B **33**, 5435 (2000).
[17] M. Klapisch, J. L. Schwob, B. S. Fraenkel, and J. Oreg, J. Opt. Soc. Am. **67**, 148 (1977).
[18] M. F. Gu, Astrophys. J. **582**, 1241 (2003).
[19] K. Yamakawa *et al.*, Opt. Lett. **23**, 1468 (1998).
[20] K. Yamakawa and C. P. J. Barty, IEEE J. Sel. Top. Quantum Electron. **6**, 658 (2000).
[21] Y. Fukuda *et al.*, Pis'ma Zh. Eksp. Teor. Fiz. **78**, 146 (2003) [JETP Lett. **78**, 115 (2003).]

[22] A. S. Boldarev *et al.*, Pis'ma Zh. Eksp. Teor. Fiz. **73**, 583 (2001) [JETP Lett. **73**, 514 (2001)].
[23] F. Dorchies, F. Blasco, T. Caillaud, J. Stevefelt, C. Stenz, A. S. Boldarev and V. A. Gasilov Phys. Rev. A **68**, 023201 (2003).
[24] A. Ya. Faenov *et al.*, Phys. Scr. **50**, 333 (1994).
[25] I. Yu. Skobelev *et al.*, Zh. Eksp. Teor. Fiz. **108**, 1263 (1995) [JETP **81**, 692 (1995)].
[26] B. K. Young *et al.*, Rev. Sci. Instrum. **69**, 4049 (1998).
[27] G. Hölzer *et al.*, Phys. Scr. **57**, 301 (1998).
[28] S. G. Lee *et al.*, Rev. Sci. Instrum. **74**, 5046 (2003).
[29] M. Lamoureux, Adv. At., Mol., Opt. Phys. **31**, 237 (1993).
[30] R. Epstein, S. Skupsky, and J. Delettrez, J. Quant. Spectrosc. Radiat. Transf. **35**, 131 (1986).
[31] F. Rosmej, J. Quant. Spectrosc. Radiat. Transf. **51**, 319 (1994).
[32] J. Abdallah, Jr. *et al.*, Phys. Scr. **53**, 705 (1996).
[33] S. B. Hansen and A. S. Shlyaptseva, Phys. Rev. E **70**, 036402 (2004).
[34] R. C. Issac *et al.*, Phys. Plasmas **11**, 3491 (2004).
[35] S. B. Hansen, Ph.D. thesis, University of Nevada, Reno, 2003.
[36] J. Bailey *et al.*, J. Phys. B **19**, 2369 (1986).
[37] A. S. Shlyaptseva *et al.*, Phys. Rev. E **67**, 026409 (2003).
[38] S. B. Hansen *et al.*, Phys. Rev. E **70**, 026402 (2004).
[39] I. E. Golovkin *et al.*, J. Quant. Spectrosc. Radiat. Transf. **75**, 625 (2002).